ELSEVIER

Assessing potency of c-Jun N-terminal kinase 3 (JNK3) inhibitors using 2D molecular descriptors and binary QSAR methodology

Ismail Ijjaali,* François Petitet, Elodie Dubus, Olivier Barberan and André Michel

Aureus Pharma, 174 Quai de Jemmapes, Paris, France

Abstract—JNK3 signaling pathway is gaining interest due to its involvement in many neurological disorders. The purpose of this study was to explore for the first time the use of a large and diverse dataset in combination with binary QSAR methodology for predicting JNK3 activity class. Data were extracted from Aureus Pharma' AurSCOPE Kinase knowledge database and active or inactive classes were assigned to ligands based on IC_{50} biological activity. Two sets of 2D molecular descriptors (P_VSA and BCUT) were used to build models using different biological activity thresholds. The design of the models was preceded by the evaluation of the chemical space covered by the datasets and an assessment of its chemical diversity. The best model was found using a 100 nM IC_{50} threshold with surface-based P_VSA descriptors. This binary QSAR model reached an overall accuracy of 98% and a leave-one-out cross-validated accuracy of 94%. Most relevant descriptors were found to encode size and hydrophobic interactions. These derived models can be useful for screening chemical libraries in the search for new JNK3 inhibitors.
© 2007 Elsevier Ltd. All rights reserved.

1. Introduction

c-Jun N-terminal kinase-3 (JNK3) is a member of the mitogen-activated protein kinase (MAP kinase) family along with JNK1 and JNK2. JNK3 has been shown to modulate neuronal apoptosis and may therefore be involved in the pathology of neurodegenerative diseases. Inhibitors of JNK3 could be useful for treating Parkinson's disease, Alzheimer's disease, epilepsy, stroke, and other dysfunctions of the central nervous system (CNS).[1,2] Therefore, development of JNK3 inhibitors has gained increasing interest, and a series of potent inhibitors have been characterized. The high level of structure homology among JNK isoforms makes the development of selective JNK3 inhibitors challenging. To address the issues of potency and selectivity, Scapin et al. reported four crystal structures of JNK3 in complex with different classes of ATP binding site inhibitors, providing more insight into the inhibitor–kinase interactions.[3] High-throughput campaigns at several laboratories considered diverse chemical classes in the search for

JNK3 inhibitors. These classes include 2-amino-4-imidazole pyrimidines, 2-aminopyrimidinyls, pyrimidinyl acetonitriles, anthrapyrazoles, thiophenyl or benzyl sulfonamides, and many other chemical series.[4] To understand JNK3 inhibitory mechanisms and elucidate pharmacophoric properties, several studies were conducted using 3D in silico approaches. Recently, 3D-QSAR (quantitative structure–activity relationships) analyses have been performed on a set of 44 benzothiazol-2-yl acetonitrile pyrimidine core derivatives using different 3D approaches.[5,6] Previously, based on a combination of hits from high-throughput screening and X-ray crystal structure information, new selective JNK3 inhibitors were designed.[7–9]

In this study, we have evaluated the suitability of 2D molecular descriptors and binary QSAR in biological activity prediction. The binary QSAR is a relatively new methodology in which biological activity is expressed in a binary format (1, active; 0, inactive).[10,11] The biological activity is correlated to molecular descriptors for a set of training compounds for which a probability distribution is computed. As a ligand-based virtual screening approach, this model can then be used to rapidly predict biological activity of new compounds. In this work, we evaluate the capability of

---

this methodology in discriminating between active and inactive JKN3 inhibitors. To the best of our knowledge, this work constitutes the first study using binary QSAR approach on JNK3 kinase.

2. Results and discussion

In this study, we have, for the first time, applied the binary QSAR approach to develop efficient predictive models of JNK3 inhibition. Such analyses require detailed and precise biological data from which the models are built. From the knowledge database developed at Aureus Pharma, high-quality datasets can be easily retrieved as was done in the present work for JNK3 target.

2.1. Chemical diversity of datasets

Prior to building binary models, the chemical diversity of JNK3 datasets was assessed using ChemAxon's proprietary chemical fingerprints (CF).[12] Chemical clustering based on these fingerprints was performed to evaluate structural representatives of the analyzed dataset. To do so, we employed a version of the Jarvis–Patrick algorithm as implemented in the Jarp algorithm of the ChemAxon's module JKlustor.[12] The output of this analysis is a number of cluster centers (centroids) and singletons at different chemical similarity thresholds. At 90% similarity threshold, 119 singletons and 36 centroids were found, with an average size of six molecules per cluster. These results illustrate the chemical diversity of the JNK3 dataset used in this analysis. Indeed, singletons represent more than 33% of the whole dataset, in addition to the small average size of obtained clusters. Furthermore, the average and maximum self-dissimilarities within the global dataset were 49.9% and 87.8%, respectively, corroborating clustering results. Figure 1 depicts some chemical representatives of JNK3 inhibitors and shows the chemical diversity of compounds analyzed.

To picture this diversity, molecules of JNK3 dataset (357 molecules) were compared with AurSCOPE Kinase database (Fig. 2a). The comparison was based on the two principal components calculated from 32 P_VSA descriptors of all the molecules. The well-distributed data for JNK3 dataset reinforce the assertion that this dataset covers a large chemical space.

2.2. Binary QSAR parameters

The accuracy of the different binary models built with different parameters, that is, varying smoothing parameter, number of components, active/inactive threshold conducted us to an optimal value of smoothing parameter of 0.01. During the model building process, the smoothing parameter is introduced to minimize the effect of bin boundaries.[10,11] Varying this parameter from 0.25 to 0.01 modifies significantly the accuracy values with an overall accuracy ranging from 76% to 98%. In addition, number of components was set to its default value meaning that the maximum of principal components was used to build binary models.

2.3. P_VSA versus BCUT molecular descriptors

Table 1 summarizes the obtained accuracies at different biological thresholds with P_VSA or BCUT descriptors. Clearly, P_VSA descriptors were more efficient than BCUT descriptors for all inhibition thresholds. Using P_VSA descriptors, the accuracy on actives ranges from 92% to 98%. The best model had an overall accuracy of 98% with an active/inactive cutoff of 100 nM (Fig. 3). The non-cross-validated predictive accuracy is 98% on inhibitors and 97% on non-inhibitors. At the same cutoff, that is, 100 nM, BCUT descriptors lead to lower but still a very satisfactory overall accuracy of 93%. P_VSA descriptors have been successfully used in many classification approaches where they demonstrated their predictive power when used with different statistical learning methods.[26,18–20]
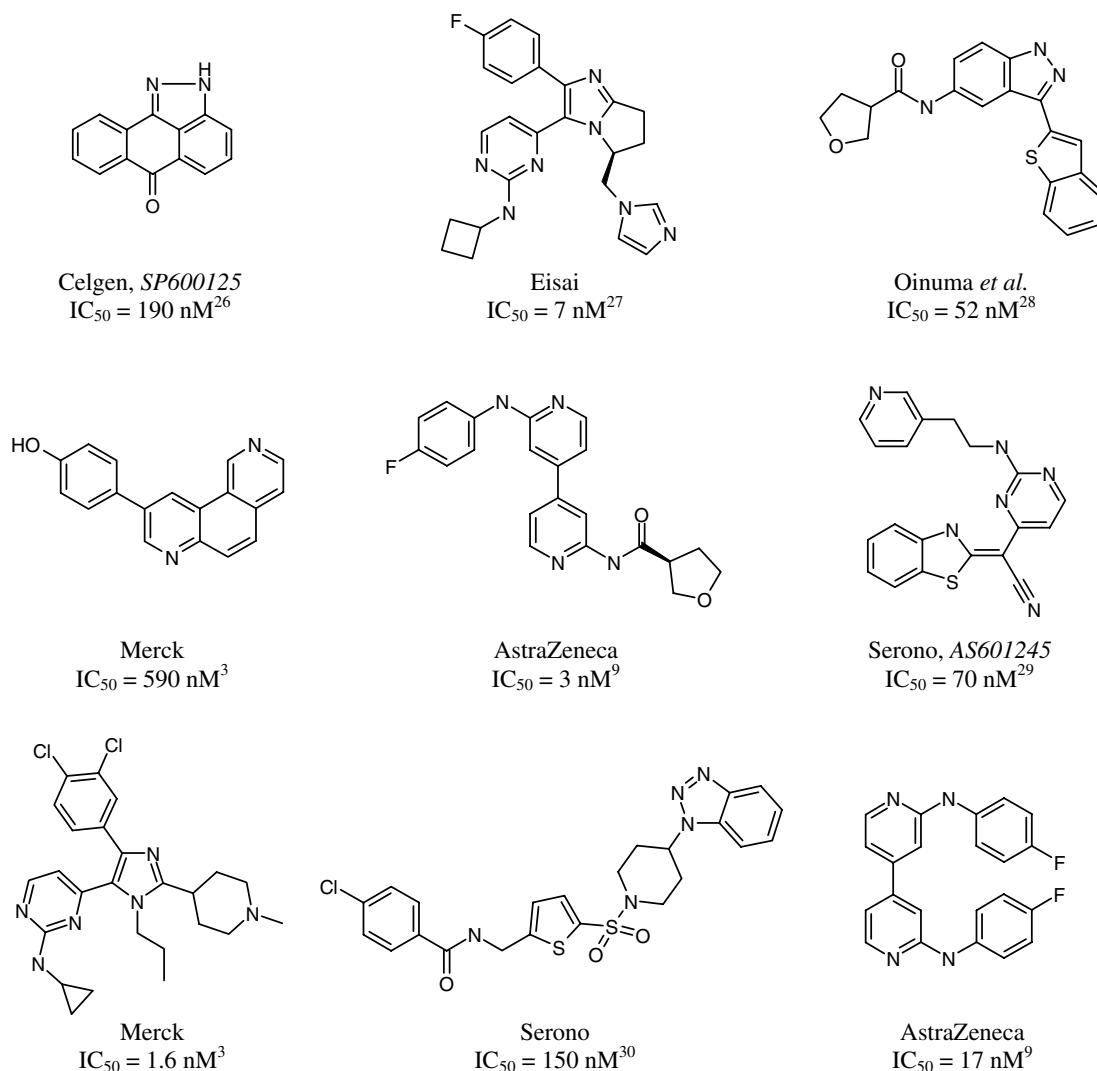
A final model was generated with the extreme classes, that is, 59 molecules having IC_{50} less than 100 nM and 97 molecules with IC_{50} greater than 1 µM. This P_VSA based model did not show a better prediction than the 100 nM model (overall accuracy of 96%) which is probably due to its limited corresponding dataset.

2.4. Models validation

To rigorously validate the predictive ability of the developed models and to confirm accuracy of the reported results we have conducted a leave-one-out (LOO) analysis. For models built using P_VSA descriptors, the LOO cross-validated overall accuracy ranges from 90% to 94%. Particularly, for the 100 nM model, the LOO cross-validated accuracy is 83% on actives and 98% on inactives.

Considering 100 nM threshold, the corresponding dataset was split into two sets: training set (50 actives, 200 inactives) and test set (9 actives, 15 inactives). The molecules were selected using the Diverse Subset algorithm implemented in MOE. This method ranks entries in a database based on their distance (similarity) from each other and is suitable to extract diverse subsets. A projection of the training and test datasets is displayed on Figure 2b. A new binary model was built with this training set which led to an overall accuracy of 96%. Based on this model, eight out of nine (89%) actives and 12 out of 15 inactives (80%) were correctly predicted leading to an overall prediction of 83%. It is worth mentioning that these misclassified have their unique reported IC_{50} far from the threshold of the model, that is, 100 nM.

The four misclassified molecules by the 100 nM model are listed in Table 2. To gain insight from these results, one should compare active and inactive molecules within congeneric structures as illustrated in Table 3. For each molecule pair, some descriptors contribute more than others in discriminating between active and inactive compounds. For example, micromolar compound **5** and nanomolar compound **6** have four identical size and hydrophilic descriptors but clearly different electrostatic descriptors. However, due to the bin nature of P_VSA descriptors, it remains difficult to translate these

Celgen, *SP600125*
IC_{50} = 190 nM[26]

Eisai
IC_{50} = 7 nM[27]

Oinuma *et al.*
IC_{50} = 52 nM[28]

Merck
IC_{50} = 590 nM[3]

AstraZeneca
IC_{50} = 3 nM[9]

Serono, *AS601245*
IC_{50} = 70 nM[29]

Merck
IC_{50} = 1.6 nM[3]

Serono
IC_{50} = 150 nM[30]

AstraZeneca
IC_{50} = 17 nM[9]

Figure 1. Selected chemical representatives of the JNK3 dataset.

values to a direct chemical meaning. Nevertheless, examination of these descriptors can help to propose different substituents around a given chemical scaffold to make resulting compounds falling into either the active or inactive range.

2.5. Comparison with 3D approaches

The three-dimensional structure of JNK3 in complex with diverse small ligands was reported by Merck researchers to elucidate the structural basis for potency and selectivity.[4] It was found that small, flat, hydrophobic molecules interact preferentially with JNK3 and afford considerable selectivity over p38 kinase. Hydrophobic and size effects were found to explain the biological potency of JNK3 inhibitors which corroborates our present findings as discussed later. Swahn et al. reported the structure-based design and synthesis of 6-aminoindazoles and 2′-anilino-4,4′-bipyridines series as selective inhibitors of JNK3.[8,9] An X-ray crystallographic study confirmed a hydrogen bonding and a basic amine-Asp electrostatic interaction. More recently, 3D-QSAR analyses were conducted to explore the bind-

ing mode of benzothiazol-2-yl acetonitrile pyrimidine core-based derivatives as potent JNK3 inhibitors.[5,6] For this class of inhibitors, these authors demonstrated that the interaction mode takes into consideration inhibitor conformation, steric, hydrophobic, and donor/acceptor electrostatic interactions.

Table 4 lists the 10 most important molecular descriptors involved in the 100 nM model. This ranking represents the contribution of each descriptor in distinguishing between actives and inactives. The average values of these descriptors for actives and inactives of JNK3 are reported in Table 4. The top five descriptors are mainly comprised of log P-based descriptors which capture the hydrophobic and hydrophilic effects. The most important descriptor SMR_VSA5 along with SMR_VSA0, SMR_VSA3, and SMR_VSA6 reflect the size and polarizability of a given molecule. Direct electrostatic interactions are expressed by PEOE_VSA-0 and PEOE_VSA+0 descriptors. It is important to note that these 2D descriptors express structural information as molecular surfaces. This is an advantage of P_VSA descriptors since molecular surface is the interface
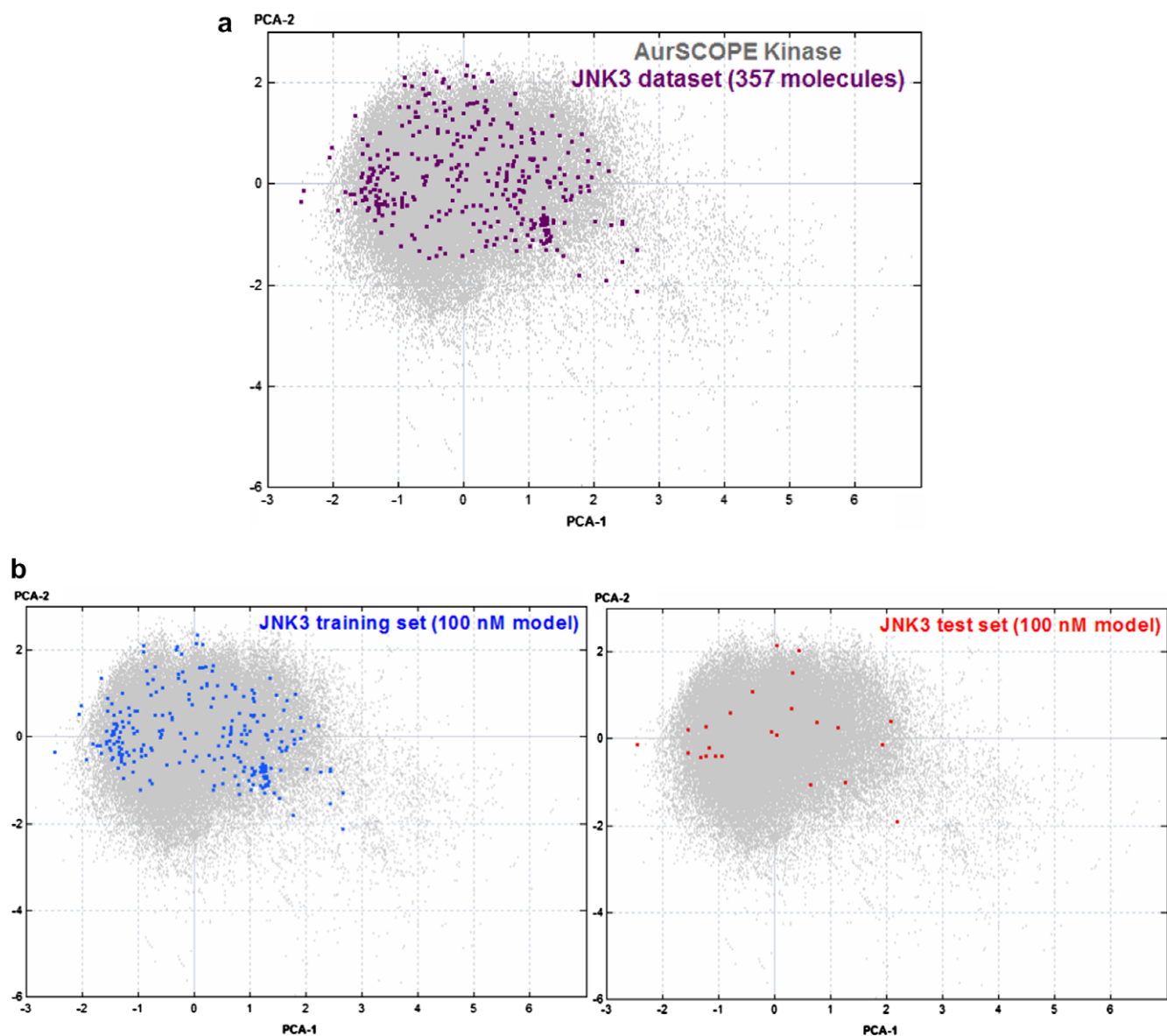
Figure 2. (a) Projection of JNK3 dataset (purple dots) within the chemical space of AurSCOPE Kinase knowledge database (gray dots) according to the first two PCA axes computed using P_VSA descriptors. (b) Projection of training (blue dots) and test (red dots) sets corresponding to the 100 nM model.

Table 1. Comparison of performance for obtained models at different inhibition thresholds using P_VSA or BCUT descriptors

Inhibition threshold (nM)	Descriptors	Accuracy on actives	Accuracy on inactives	Overall accuracy
1000 (1 μM)	P_VSA	92|87	97|94	95|91
	BCUT	84|78	84|81	84|80
500	P_VSA	96|93	93|92	94|92
	BCUT	90|84	86|83	88|83
400	P_VSA	95|92	93|89	94|91
	BCUT	91|87	80|76	86|82
300	P_VSA	96|95	93|85	94|90
	BCUT	92|88	80|76	87|83
200	P_VSA	97|95	97|86	97|92
	BCUT	95|93	85|77	92|87
100	P_VSA	98|98	97|83	98|94
	BCUT	93|92	93|83	93|90

Values after|correspond to leave-one-out cross-validated predictions.
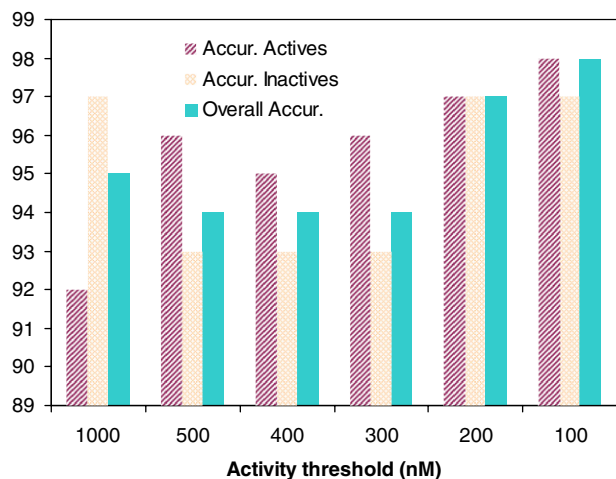
Figure 3. Overall accuracy and accuracies on actives and inactives versus the biological activity threshold.
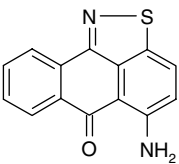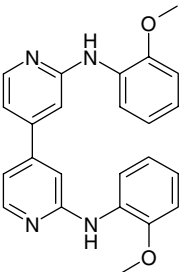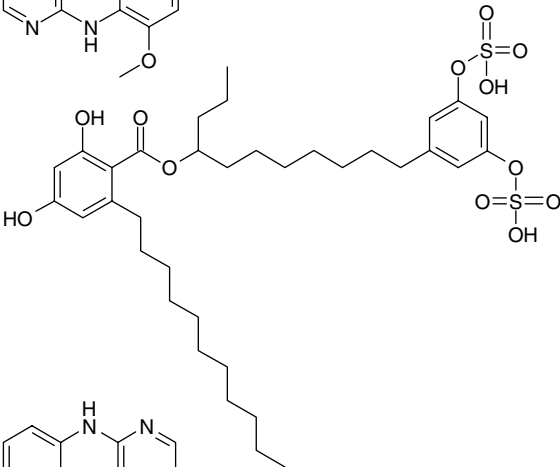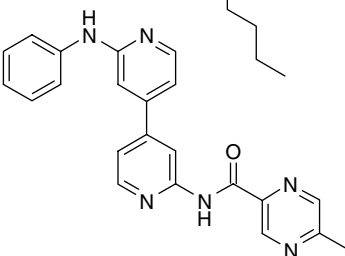
through which molecular interactions occur. However, these descriptors are hard to retro-visualize as simple chemical features to guide the chemical synthesis in an explicit way. Actually, it is impossible to evaluate the efficiency of these models compared to those obtained with other bi-dimensional approaches since to our best knowledge, this work is a first analysis using 2D surface molecular descriptors and binary QSAR method to predict JNK3 inhibition.
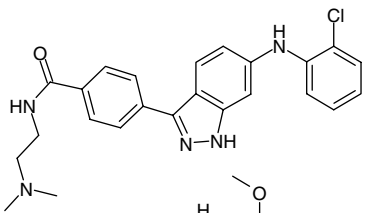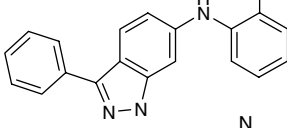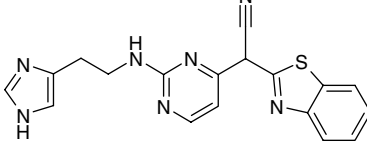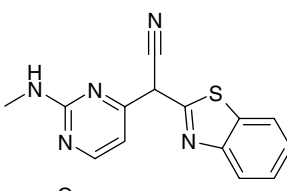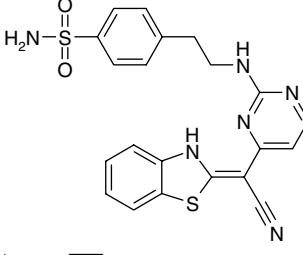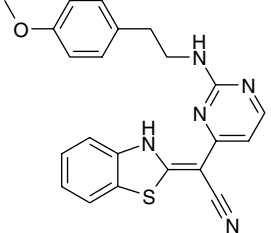
3. Conclusions

We tested the applicability of binary QSAR methodology for building binary models that use bi-dimensional molecular descriptors. Chemically diverse datasets were first extracted from AurSCOPE Kinase and methodically split into active or inactive classes via the use of the detailed biological knowledge available. Different IC_{50} thresholds were considered to analyze the boundary effect, and the best model was built with the 100 nM dataset. van der Waals surface based descriptors P_VSA were found to be more efficient than BCUT descriptors and reached an overall accuracy of 98%. The most important descriptors revealed the primary contribution of hydrophobic and size effects in addition

Table 2. Misclassified JNK3 compounds using 100 nM model

Molecule	IC_{50} (nM)	Class	Prediction
	400	(0)	(1)
	528	(0)	(1)
	500	(0)	(1)
	33	(1)	(0)

Table 3. Selected active and inactive molecules having similar chemical scaffold along with their corresponding molecular descriptors

Molecule	IC$_{50}$	Molecular descriptors					
		SMR_VSA5	$S\log P$_VSA7	$S\log P$_VSA8	$S\log P$_VSA3	$S\log P$_VSA9	PEOE_VSA+0
1	1.9 nM	194.1	208.2	0	36.9	44.7	89.1
2	202 nM	211.7	222.4	0	0	10.8	36.1
3	70 nM	158.3	142.3	0	66.1	33.2	81.1
4	950 nM	105.4	108.3	0	47.7	33.2	38.2
5	41 nM	194.9	179.2	0	66.1	36.9	109.7
6	3.1 μM	194.9	179.2	0	66.1	42.1	82.9

Table 4. Top 10 important P_VSA descriptors involved in the 100 nM model

P_VSA descriptors	Chemical meaning	Average value	
		Actives	Inactives
SMR_VSA5	Size	217.4	190.9
SlogP_VSA7	Hydrophobic	187.9	155.0
SlogP_VSA8	Hydrophobic	32.2	28.3
SlogP_VSA3	Hydrophobic	35.5	40.8
SlogP_VSA9	Hydrophobic	45.9	89.0
PEOE_VSA+0	Electrostatic	87.3	85.9
SMR_VSA6	Size	34.2	31.9
SMR_VSA0	Size	31.4	49.9
PEOE_VSA-0	Electrostatic	92.6	72.2
SMR_VSA3	Size	8.0	12.4

For each descriptor the average values for active and inactive compounds are reported.

to electrostatic interactions in accordance with previous 3D structure-based studies.

In conclusion, combining rapid computational approaches such as binary QSAR and precise biological knowledge resources can assist efficiently high-throughput screening campaigns and may be used as preliminary filtering step in drug design process.

4. Experimental

4.1. Dataset extraction

The training sets used for models generation have been extracted from the Aureus Kinase knowledge

database.[21] This database covers biological data published on kinases and provides chemical structures information, references to the original publication or patent, and detailed information on experimental conditions. Figure 4 illustrates the principal components-based chemical space of AurSCOPE Kinase compared with the known NCI database[22] demonstrating the large chemical diversity of the Kinase knowledge database. The two principal components were computed using P_VSA descriptors (see Section 4.2).

To retrieve all the analyzed datasets, we used the query software developed by Aureus. This tool allows for the interrogation of knowledge databases and the extraction of all pertinent chemical and biological information regarding a specific target under defined conditions. For this work, a series of compounds tested in enzymology inhibition experiments on the wild type JNK3 kinase have been selected. Only wild-type targets were considered; fragment or mutated targets were unretained. This first selection retrieved 558 molecules associated with 592 biological activities, coming from 21 articles and 30 patents (June 2006 database release). A distribution of these activities based on different biological parameters is given in Figure 5. We then selected 357 unique molecules having, at least, a measured IC$_{50}$ value. Two hundred thirty-one and 126 molecules are associated with exact and modulated IC$_{50}$ values, respectively. While we retrieved datasets

using supplementary biological filters, that is, the binding action site, species, cell line, this resulted in very restricted and unbalanced datasets which could not be adequately used in the current study. Finally, we considered all 357 molecules to build different binary models.

In binary QSAR methodologies, before building models we need to define a biological activity threshold and assign active or inactive categories to compounds under study. Number of actives and inactives differs depending on inhibition threshold expressed by IC$_{50}$. To examine the effect of threshold on model performance, exact and modulated IC$_{50}$ values were meticulously examined to constitute a variety of datasets. This resulted in six different datasets with inhibition thresholds: 1 μM, 500 nM, 400 nM, 300 nM, 200 nM, and 100 nM. Table 5 shows the dataset profiles at each of these different threshold values. Note that for some thresholds, the total number of actives and inactives does not correspond to the initial number of molecules, that is, 357 since it was impossible to assign a biological category to molecules that are associated with modulated or range activities. Next, for each dataset, the performances of QSAR binary models were evaluated and compared.

4.2. Computation

The chemical structures were exported along with associated biological activities as SD files that were loaded
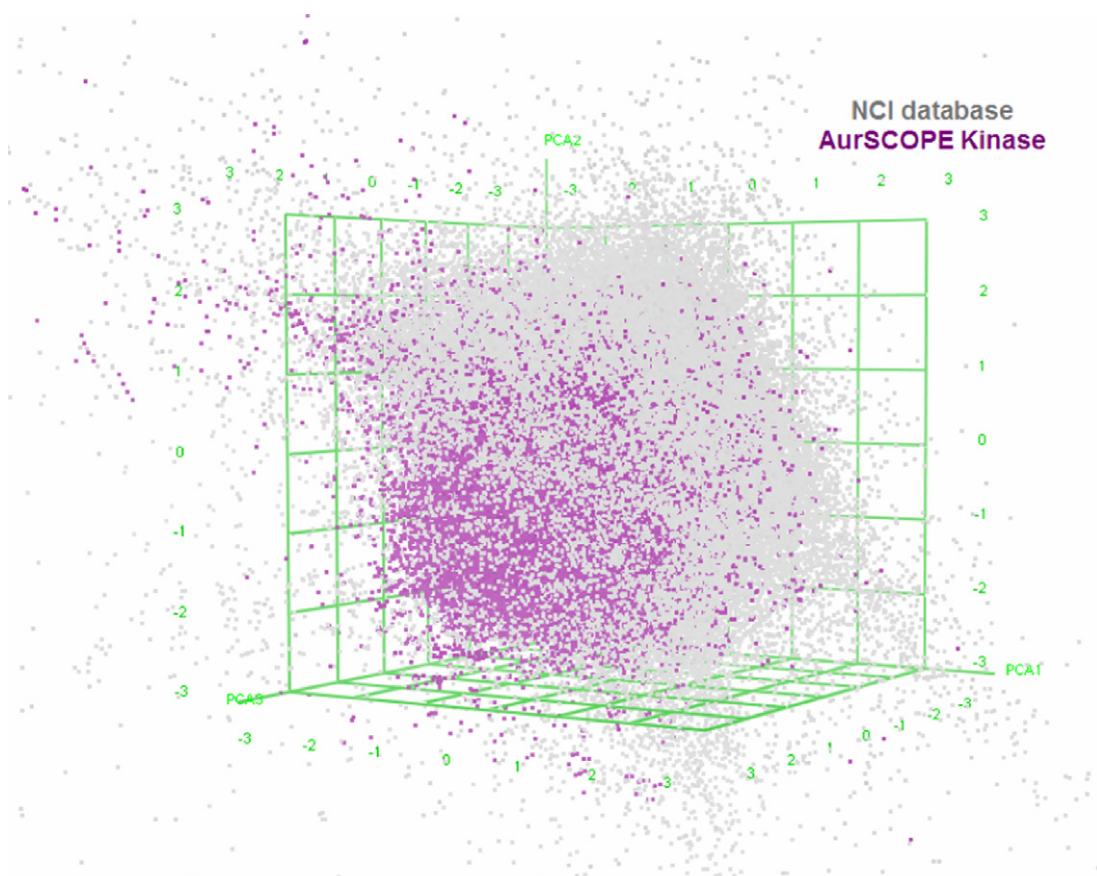
Figure 4. Distribution of AurSCOPE Kinase database (purple dots) compared to the NCI database (gray dots). The comparison is based on the three first principal components computed from 32 P_VSA descriptors.
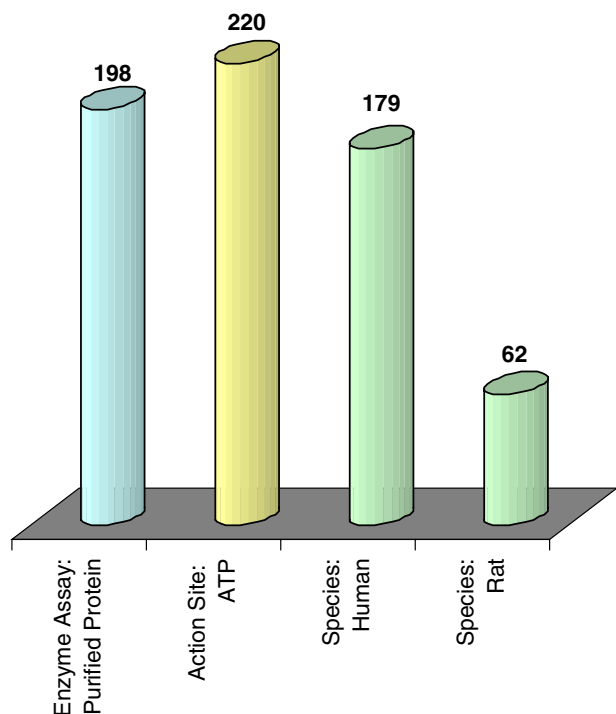
Figure 5. Activities distribution based on different biological filters for the entire wild-type JNK3 dataset.

Table 5. Actives and inactives distribution at different biological threshold values

Threshold value IC$_{50}$ (nM)	Inhibitors classification	
	Actives	Inactives
1000	207	97
500	158	136
400	136	147
300	123	160
200	96	188
100	59	215

into cheminformatic tools for subsequent calculations. Managing all data, calculating descriptors, building binary QSAR models, and predicting the classes were all executed on a Microsoft Windows XP computer (3 GHz CPU, 1 GB RAM).

4.2.1. Binary QSAR. Binary QSAR was developed by P. Labute and implemented in the MOE (Molecular Operating Environment) suite.[10,11,23] it is based on Bayesian inference technique, which is used to classify a compound as active or inactive on the basis of its associated molecular descriptors. A detailed description of the binary QSAR methodology has been introduced in previous publications and briefly described hereafter.[24–27]

This qualitative technique estimates the probability density $\Pr(Y = 1|X = x)$, where Y is a binary variable ($Y = 1$ for JNK3 actives, $Y = 0$ for JNK3 inactives) and X is an n-vector containing the descriptors values of molecules for which we want to predict the class activity. The ori-

ginal molecular descriptors of the training set are transformed using principal components analysis (PCA) to obtain a decorrelated and normalized set of descriptors. A *smoothing factor* σ is introduced to reduce the effect of bin boundaries.[11]

The quality of a binary QSAR model is measured using a normal validation and the cross-validation procedure. The three parameters are (1) accuracy on inactive compounds, $c0/m0$; (2) accuracy on active compounds, $c1/m1$; (3) overall accuracy on all of the compounds, $(c0 + c1)/(m0 + m1)$, where $m0$ is the number of inactive compounds, $m1$ the number of active compounds, $c0$ the number of inactive compounds correctly predicted by the QSAR model, and $c1$ the number of active compounds correctly predicted. The derived binary QSAR model is cross-validated by the leave-one-out (LOO) procedure. In this procedure, only one molecule is eliminated at a time using the rest to build the model and the process is repeated until all molecules have been eliminated once. Accuracy is calculated for each step, and an average accuracy for all the steps is reported as a measure of the internal predictivity of the model within the training set.

4.2.2. Molecular descriptors generation. In this analysis, two sets of molecular descriptors were used: 2D surface descriptors P_VSA and Burden eigenvalues BCUT descriptors. 32 P_VSA molecular descriptors were computed using MOE.[23] These descriptors are reported to be implicitly linked to ligand binding and express various physicochemical properties (lipophilic, pharmacophoric, steric, and electronic) in terms of van der Waals surface.[28]

Using DRAGON software, 64 Burden eigenvalues (BCUT) were computed on hydrogenized structures[29] and then imported into MOE for models building. Based on PCA, only 11 uncorrelated BCUT descriptors were considered to build binary models. BCUT descriptors incorporate both connectivity information and atomic properties (atomic charge, polarizability, and hydrogen bond abilities) relevant to intermolecular interactions.[25,30–33]

References and notes

1. Kyriakis, J. M.; Avruch, J. *Physiol. Rev.* **2001**, *81*, 807.
2. Zhang, G. Y.; Zhang, Q. G. *Expert Opin. Invest. Drugs* **2005**, *14*, 1373.
3. Scapin, G.; Patel, S. B.; Lisnock, J. M.; Becker, J. W.; LoGrasso, P. V. *Chem. Biol.* **2003**, *10*, 705.

4. Resnick, L.; Fennell, M. *Drug Discov. Today* **2004**, *9*, 932, and references therein.
5. Sharma, P.; Ghoshal, N. *J. Chem. Inf. Model.* **2006**, *46*, 1763.
6. Shaikh, A.R.; Ismael, M.; Del Caprio, C.A.; Tsuboi, H.; Koyama, M.; Endou, A.; Kubo, M.; Broclawik, E.; Miyamoto, A. *Bioorg. Med. Chem. Lett.* **2006**, in press.
7. Stocks, M. J.; Barber, S.; Ford, R.; Leroux, F.; St-Gallay, S.; Teague, S.; Xue, Y. *Bioorg. Med. Chem. Lett.* **2005**, *15*, 3459.
8. Swahn, B. M.; Huerta, F.; Kallin, E.; Malmström, J.; Weigelt, T.; Viklund, J.; Womack, P.; Xue, Y.; Öhberg, L. *Bioorg. Med. Chem. Lett.* **2005**, *15*, 5095.
9. Swhan, B. M.; Xue, Y.; Arzel, E.; Kallin, E.; Magnus, A.; Plobeck, N.; Viklund, J. *Bioorg. Med. Chem. Lett.* **2006**, *16*, 1397.
10. Labute, P. *Proc. Pacific Symp. Biocomput.* **1999**, 444.
11. Labute, P.; Nilar, S.; Williams, C. *Comb. Chem. High Throughput Screen.* **2002**, *5*, 135.
12. JChem, version 3.1.7, ChemAxon, 1037 Budapest, Hungary, http://www.chemaxon.com.
13. Bennett, B. L.; Sasaki, D. T.; Murray, B. W.; O'Leary, E. C.; Sakata, S. T.; Xu, W.; Leisten, J. C.; Motiwala, A.; Pierce, S.; Satoh, Y.; Bhagwat, S. S.; Manning, A. M.; Anderson, D. W. *Proc. Nat. Acad. Sci. U.S.A.* **2001**, *98*, 13681.
14. Graczyk, P.; Numata, H.; Khan, A.; Palmer, V.; Medland, D.P.; Oinuma, H.; Bhatia, G. Eisai Co, Patent WO 02/081475 A1, 2002.
15. Oinuma, H.; Ohi, N.; Sato, N.; Soejima, M.; Seshimo, H.; Terauchi, T.; Doko, T.; Kohmura, N. Patent US 2005/0282880 A1, 2005.
16. Carboni, S.; Hiver, A.; Szyndralewiez, C.; Gaillard, P.; Gotteland, J. P.; Vitte, P. A. *J. Pharmacol. Exp. Ther.* **2004**, *310*, 25.
17. Ruckle, T.; Biamonte, M.; Grippi-Vallotton, T.; Arkinstall, S.; Cambet, Y.; Camps, M.; Chabert, C.; Church, D. J.; Halazy, S.; Jiang, X.; Martinou, I.; Nichols, A.; Sauer, W.; Gotteland, J. P. *J. Med. Chem.* **2004**, *47*, 6921.
18. Dubus, E.; Ijjaali, I.; Petitet, F.; Michel, A. *ChemMedChem* **2006**, *1*, 622.
19. Burton, J.; Ijjaali, I.; Barberan, O.; Petitet, F.; Vercauteren, D. P.; Michel, A. *J. Med. Chem.* **2006**, *49*, 6231.
20. Klon, A. E.; Lowrie, J. F.; Diller, D. J. *J. Chem. Inf. Model.* **2006**, *46*, 1945.
21. Aureus Pharma, Paris, 75010, France, http://www.aureuspharma.com.
22. NCI database, version 2000, http://cactus.nci.nih.gov/ncidb2/download.html.
23. MOE, Chemical Computing Group Inc., Montreal, H3A 2R7 Canada, http://www.chemcomp.com.
24. Gao, H.; Williams, C.; Labute, P.; Bajorath, J. *J. Chem. Inf. Comput. Sci.* **1999**, *39*, 164.
25. Gao, H. *J. Chem. Inf. Comput. Sci.* **2001**, *41*, 402.
26. Baurin, N.; Mozziconacci, J.-C.; Arnoult, E.; Chavatte, P.; Marot, C.; Morin-Allory, L. *J. Chem. Inf. Comput. Sci.* **2004**, *44*, 276.
27. Prathipati, P.; Saxena, A. K. *J. Chem. Inf. Model.* **2006**, *46*, 39.
28. Labute, P. *J. Mol. Graph. Model.* **2000**, *18*, 464.
29. Todeschini, R.; Consonni, V.A.; Mauri, M.P.; Talete srl, Milano, Italy, http://www.disat.unimib.it/chm/.
30. Burden, F. R. *J. Chem. Inf. Comput. Sci.* **1989**, *29*, 225.
31. Pearlman, R. S.; Smith, K. M. *J. Chem. Inf. Comput. Sci.* **1999**, *39*, 28.
32. Stanton, D. T. *J. Chem. Inf. Comput. Sci.* **1999**, *39*, 11.
33. Pirard, B.; Pickett, S. D. *J. Chem. Inf. Comput. Sci.* **2000**, *40*, 1431.